Conformational analysis and vibrational study of daidzein by using FT-IR and FT-Raman spectroscopies and DFT calculations

ARTICLE *in* SPECTROCHIMICA ACTA PART A MOLECULAR AND BIOMOLECULAR SPECTROSCOPY · OCTOBER 2013

Impact Factor: 2.35 · DOI: 10.1016/j.saa.2013.10.045 · Source: PubMed

7 AUTHORS, INCLUDING:

Harshita Singh
University of Lucknow
3 PUBLICATIONS **7** CITATIONS
SEE PROFILE

Dr. Anubha Srivastava
University of Lucknow
22 PUBLICATIONS **111** CITATIONS
SEE PROFILE

Poonam Tandon
University of Lucknow
206 PUBLICATIONS **986** CITATIONS
SEE PROFILE

Sudhir Kumar
Central Drug Research Institute
8 PUBLICATIONS **14** CITATIONS
SEE PROFILE

Spectrochimica Acta Part A: Molecular and Biomolecular Spectroscopy 120 (2014) 405–415

Contents lists available at ScienceDirect

Spectrochimica Acta Part A: Molecular and Biomolecular Spectroscopy

journal homepage: www.elsevier.com/locate/saa

Conformational analysis and vibrational study of daidzein by using FT-IR and FT-Raman spectroscopies and DFT calculations

Harshita Singh [a], Swapnil Singh [a], Anubha Srivastava [a], Poonam Tandon [a,*], Purnima Bharti [a], Sudhir Kumar [b], Rakesh Maurya [b]

[a] Department of Physics, University of Lucknow, Lucknow 226007, India
[b] Medicinal and Process Chemistry Division, Central Drug Research Institute (CDRI), Lucknow 226031, India

HIGHLIGHTS

- FT-IR and FT-Raman data were recorded and computed with the theoretical results.
- Computations were performed on the most stable conformer of daidzein.
- NBO analysis was performed to elucidate the charge delocalization properties.
- NLO study reveals the nonlinearity of the molecule.
- UV–Vis study predict the electronic excitations by using TD-DFT/6-31G method.

GRAPHICAL ABSTRACT

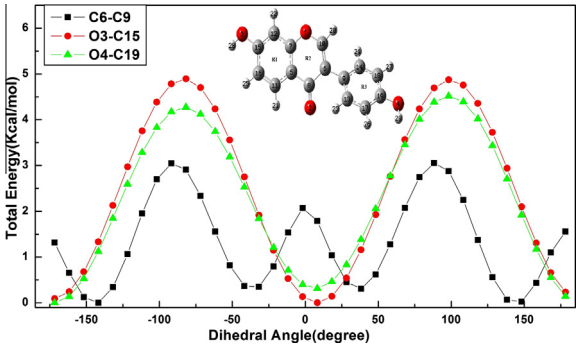

ARTICLE INFO

Article history:
Received 19 August 2013
Received in revised form 2 October 2013
Accepted 9 October 2013
Available online 19 October 2013

Keywords:
Daidzein
IR and Raman spectroscopy
NBO analysis
NLO
HOMO–LUMO
DFT

ABSTRACT

Daidzein ($C_{15}H_{10}O_4$) is a type of isoflavone. It was isolated from *Butea monosperma* that belongs to the Fabaceae family. Soybeans and soy products are the abundant source of daidzein. It is the subject of investigation for many reasons, as it has got wide applications, such as anti-tumor, anti-estrogen, weak pro-estrogen and anti-cancer activities.

In the present study, a complete vibrational assignment is provided for the observed IR and Raman spectra of daidzein. Electronic properties have been analyzed using TD-DFT method for both gaseous and solvent phase. The optimized geometry, total energy, potential energy surface and vibrational wavenumbers of daidzein have been determined using density functional theory (DFT/B3LYP) method with 6-311++G(d,p) basis set and a good correlation was found between observed and calculated values. The double well potential energy curve of the molecule about three bonds, has been plotted, as obtained from DFT/6-31G basis. The HOMO–LUMO energy gap of possible conformers has been calculated for comparing their chemical activity. Global reactivity descriptors have been calculated for predicting the chemical reactivity and the stability of chemical systems. Electrostatic potential surface has been plotted for predicting the structure activity relationship. NBO analysis has also been performed to study the stability of the molecule. NLO study reveals the nonlinear properties of the molecule. ^1H and ^{13}C NMR spectra have also been studied. Finally, the calculated results were used to simulate infrared and Raman spectra of the title compound which showed a good agreement with the observed spectra.

Introduction

Daidzein (7,4′-dihydroxyisoflavone) is the type of isoflavone, isolated from *Butea monosperma* [1], belongs to the family of Fab-

* Corresponding author. Tel.: +91 522 2782653; fax: +91 522 2740840.
E-mail addresses: poonam_tandon@hotmail.com, poonam_tandon@yahoo.co.uk (P. Tandon).

1386-1425/$ - see front matter © 2013 Elsevier B.V. All rights reserved.
http://dx.doi.org/10.1016/j.saa.2013.10.045

aceae which is popularly known as Flame of forest, Dhak, Palas or Bastard teak. It is mainly found in soybeans and soy products as well as in other species of Fabaceae family such as beans, peas, nuts, grain products, coffee, tea and certain herb like red clover [2]. Daidzein is also called phytoestrogen because it shares similar structure and function with mammalian endogenous harmone estrogen [3]. This quality made it useful for a range of estrogen dependent diseases, such as breast cancer, menopausal symptoms, cardiovascular disease and osteoporosis [4,5]. *In vitro* and *in vivo* studies reveals that, daidzein is highly active antioxidant and plays an important role in anti-estrogenic [6–9], anticancer [10–13], anti-inflammatory [14–16], cardioprotective [17,18] and enzyme-inhibitory effects [19–21].

Daidzein is a lipophilic substance, thus it is able to pass through the placental barrier and this demonstrated that feeding pregnant sows with a daidzein-supplemented diet improved pre- and post-natal growth in newborn male piglets [22,23]. It also exerts significant neuronal protection and neuritogenic effects for a variety of cultured neuronal cells, e.g. hippocampal neurons, cortical neurons, dorsal root ganglion neurons, and PC12 cells [24–27].

Vibrational spectroscopy is an analytical tool for providing information about structure, composition, conformation and intramolecular interactions of complex molecules [28,29]. It can also provide important information about relationship between molecular architecture and nonlinear response (hyperpolarizability) [30–34].

In the present paper a systematic spectroscopic and quantum chemical study of the possible conformations, their relative stabilities have been performed. The double well potential energy curves of the molecule around three bonds, have been plotted, as obtained from DFT/6-31G basis set. The optimized geometry, wavenumber and intensity of the vibrational bands of possible conformers were obtained by density functional theory (DFT) [35] employing B3LYP using 6-311++G(d,p) basis set. The calculated infrared and Raman spectra is compared with the observed Fourier transform (FT)-Raman and FT-IR spectra. Detailed assignments of the vibrational spectra have been made with the aid of theoretically predicted vibrational frequencies. Further, the NMR spectra is computed and used to interpret the ^{1}H and ^{13}C NMR spectra of daidzein reported by Pelter et al. [36].

A comparison is made between the UV–Vis spectra recorded in methanol solution and the earlier reported one [37]. The electronic absorption spectra has been calculated using time dependent-density functional theory (TD-DFT) [38,39] with 6-31G basis set and solvent effect has been introduced by integral equation formalism-polarizable continuum model (IEF-PCM) method [40,41]. The HOMO (H)-LUMO (L) energy gaps of possible conformers have been calculated for comparison of their chemical activity. Molecular electrostatic potential (MEP) surface has been plotted for predicting the structure activity relationship. Natural bond orbital (NBO) analysis has been performed to study the stability and intramolecular charge transfer (ICT) within the molecule [42,43]. Nonlinear optical (NLO) analysis has also been done to calculate first hyperpolarizability. Mulliken population analysis on atomic charges of various conformers has been performed. Global reactivity descriptors such as chemical potential (μ), electronegativity (χ), hardness (η), softness (S), global philicity (ω), H–L and their band gap (ΔE) have also been calculated. These descriptors are very important in predicting the chemical reactivity, selectivity, stability and reaction path of chemical systems. Parameters χ, μ, η and ω are used to discuss the reactive behavior of one single molecule or a set of related molecules. These descriptors have been used qualitatively to characterize reactivity of a molecule in chemical reaction. Reactivity to specific agents, e.g. electrophilic, nucleophilic or radical can be described qualitatively using the above descriptors [44,45]. In the present work we have used global reactivity descriptors to compare the relative activity of different conformers.

Experimental details

The daidzein in powder form was extracted from *Butea monosperma*. The plant material (5.5 kg) were pulverized and extracted with ethanol (4 × 25 L) at room temperature. The solvent was removed under reduced pressure to give a brown viscous extract (380 g). An aliquot of the extract (300 g) was triturated with hexane (15 × 500 ml) and chloroform (10 × 400 ml) successively, the residue was suspended in minimum amount of water (800 ml), extracted with n-butanol saturated with water (14 × 300 ml). The solvent was removed under reduced pressure to afford hexane fraction (15.0 g), chloroform fraction (15.5 g), butanol fraction (124.0 g) and aqueous fraction (206.5 g).

Part of the butanol fraction (80.0 g) was further purified over silica gel column by elution with $CHCl_3$ and MeOH as binary mixture of increasing polarity to give 61 fractions, which were combined in eight resulting fractions (F10-F17) according to thin layer chromatography (TLC) analysis. Column chromatography of fraction 14 (2.66 g) over silica gel using $CHCl_3$–MeOH (90:10) mixture afforded slightly impure compound, which was then crystallized in ethanol to afford pure colorless crystals of daidzein (70 mg) [1].

Infrared spectra were recorded on a Bruker TENSOR 27 FT-IR spectrometer with a spectral resolution of 4 cm^{-1} in the region 400–4000 cm^{-1}. KBr pellets of solid samples were prepared from mixtures of KBr and the sample in 200:1 ratio using a hydraulic press. Multi-tasking OPUS software was used for base line corrections.

The FT-Raman spectra were recorded on a Bruker multiRAM with Raman attachment which uses a 1064 nm Nd-YAG laser line as the excitation line for recording the Raman spectra in the region 100–3400 cm^{-1}. The samples were measured in the hemispheric bore of an aluminum sample holder. The spectral resolution of this instrument was also 4 cm^{-1}. Typical spectra were acquired with 512 scans and a laser power of 500mW at the sample location.

The absorption spectrum of daidzein was recorded in methanol solvent in the range 200–800 nm using a Varian Cary 50, UV–visible spectrophotometer.

Computational details

The optimized geometries and total energies of the different conformers of daidzein molecule were computed employing the DFT [35] using Gaussian 09 program package [46] and Becke's three parameter (local, non-local, HF) with Lee– Yang–Parr hybrid correlation functional (B3LYP) [47–49]. The basis set 6-311++G(d,p) augmented by 'd' polarization functions on heavy atoms and 'p' polarization functions on hydrogen atoms were used [50,51]. The wavenumber calculations were performed for all the conformers and positive wavenumber for each normal mode confirm the stability of the molecular structure obtained with minimum energy. The normal mode analysis was performed and the potential energy distribution (PED) was calculated along the internal coordinates using localized symmetry [52,53]. For this purpose a complete set of 81 internal coordinates were defined using Pulay's recommendations [52]. The vibrational assignments of the normal modes were made on the basis of the PED calculated by using the program GAR2PED [54]. Visualization and confirmation of calculated data were done by using the CHEMCRAFT program [55]. Finally the calculated normal mode vibrational wavenumbers provide spectroscopic properties also through the principles of statistical mechanics [56]. The graphical presentation of the

calculated Raman and IR spectra were made using GaussView 05 program [57]. Isoelectronic molecular electrostatic potential surfaces (ESP) were calculated and plotted for the molecule using the GaussView 05 program [57]. ^{1}H and ^{13}C NMR chemical shifts are calculated with GIAO approach [58] by applying B3LYP/6-311G(d,p) method. ^{1}H and ^{13}C isotropic magnetic shielding (IMS) of any X atom (carbon or hydrogen) were made according to the value TMS $\delta^{X} = \delta^{TMS} - \delta^{C}$ [59,60]. In order to obtain the calculated results comparable with the experimental data, we have transformed the absolute shielding returned by the program in chemical shifts by subtracting it from the absolute shielding of tetramethylsilane (TMS).

Results and discussion

Conformational studies

Initial geometrical optimization was done by using standard geometrical parameters and then by the energy minimization as shown in the Supplementary Fig. S1. In order to investigate the possible conformers of daidzein, potential energy scans were performed along the dihedral angles D1 (C10–C6–C9–C13), D2 (H28–03–C15–C12) and D3 (H29–O4–C19–C18) at the B3LYP/6-31G level of theory. The scans were obtained by minimizing the potential energy in all geometrical parameters by varying the torsion angles at a step of 10° in the range of 0–360° rotation around the bond. The variation of potential energy as a function of dihedral angle for all the three bonds is illustrated in Supplementary Figs. S2(a), S2(b) and S2(c). Total 16 conformers were obtained by the combination of potential energy scans around D1–D2 and D1–D3 and optimized at the B3LYP/6-311++G(d,p). On account of similar dihedral angles, 4 pairs of conformer are similar so we have selected only one of them and finally remaining 12 conformers are studied (shown in Supplementary Table S1 with their name). Among these, the energy of conformers C1 and A1 is lower than others and conformer C1 has minimum energy as compare to all the other conformers. So the present work is based on these two conformers. The energy difference between conformer A1 and conformer C1 is lower than kT (at room temperature) so, conformers C1 and A1 may co-exist at room temperature.

Geometry optimization and energies

The molecular structures of different conformations of title compound in the ground state are optimized with B3LYP/6-311++G(d,p) basis set and vibrational frequencies for these optimized structures have been calculated. The ground state optimized structures of conformers C1 and A1 are shown in Fig. 1(a and b), respectively. The optimized structures of the conformers C1 and A1 were compared by superimposing them using a least squares algorithm that minimizes the distances of the corresponding non-hydrogen atoms as shown in Supplementary Fig. S3. They perfectly overlapped each other due to the simultaneous rotation of ring R3 as well as hydroxyl group of the same ring, however, they have different geometries as can be seen from Fig. 1(a and b). After completion of the geometrical optimization, the total energies of the conformers C1 and A1 are found to be −878.7490044 and −878.7489889 Hartree, respectively. Therefore, conformer C1 is more stable than the conformer A1. The population ratio among the different conformers of daidzein can be calculated from the energies of the minima using Boltzmann factor, which is the simplest way of relating the energy differences to population differences and can be expressed as $\exp(-E_A/RT)$ or $\exp[-(E_1 - E_2)/k_BT]$. The population ratio of the conformers C1 and A1 was obtained to be 50.18% and 49.82%, respectively. The optimized

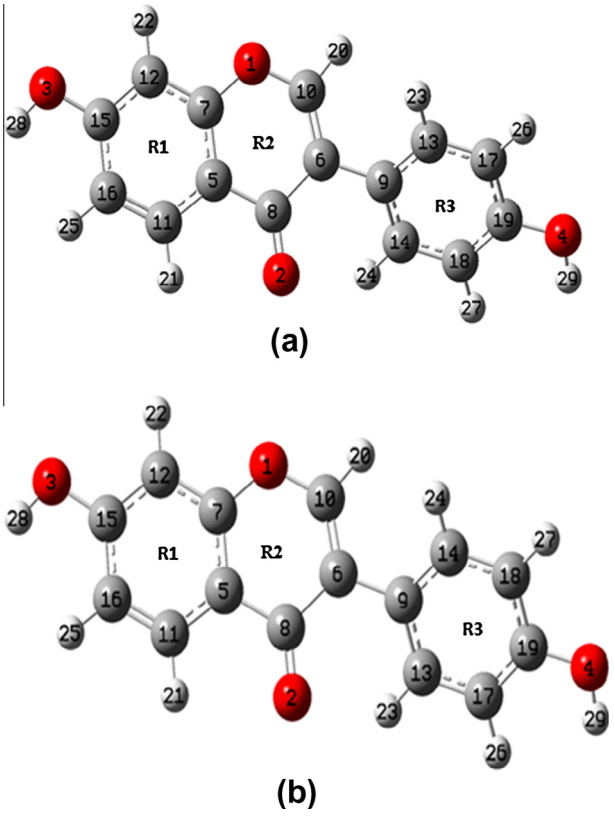

Fig. 1. (a) Optimized structure of conformers C1 and (b) A1.

structural parameters of both the conformers (bond lengths, bond angles, dihedral angles) have been compared and are listed in Table 1. From the optimized geometrical data of the conformers, it is observed that the C–C bond distances calculated between the ring carbon atoms and the C–H, O–H and C–O bond lengths are found to be nearly the same for conformers C1 and A1. It may be seen that for both the conformers C1 and A1, the DFT methods yield comparable geometries, which differ not more than 0.004 Å in bond length, 0.80° in bond angle, except the angles O4–C19–C17, O4–C19–C18, C14–C18–H27 and C13–C17–H26 which differ by 5.2°, 5.19°, 1.44° and 1.46°. Similarly the dihedral angles H29–O4–C19–C17, H29–O4–C19–C18, C8–C6–C9–C13, C8–C6–C9–C14, C10–C6–C9–C13 and C10–C6–C9–C14 have changes from 178.99° to −0.47°, −0.45° to 178.91°, −141.23° to 38.94°, 39.97° to −141.10°, 38.23° to −141.77° and −140.56° to 38.19° in going from conformer C1 to A1. The variation in these dihedral angles is only associated with the C6–C9 and O4–C19 bond which can also be seen from Fig. 1(a and b).

Molecular electrostatic potential

The molecular electrostatic potential (MEP) at a point r in the space around a molecule (in atomic units) can be expressed as:

$$V(r) = \sum_{A} \frac{Z_A}{|\vec{R}_A - \vec{r}|} - \int \frac{\rho(\vec{r}')dr'}{|\vec{r}' - \vec{r}|}$$

where Z_A is the charge on nucleus A, located at R_A and $\rho(r')$ is the electronic density function for the molecule. The first and second terms represent the contributions to the potential due to nuclei and electrons, respectively. $V(r)$ is the resultant at each point r, which is the net electrostatic effect produced at the point r by both the electrons and nuclei of the molecule. The molecular electrostatic potential (MEP) serves as a useful quantity to explain hydro-

Table 1
Comparision of geometrical parameters of daidzein.

Parameters	Optimized	Conformer C1	Conformer A1	Parameters	Optimized	Conformer C1	Conformer A1
Bond length (A)				A(C19–C18–H27)	119.21	120.02	119.22
R(O1–C7)	1.367	1.367	1.366	A(O4–C19–C17)	122.72	117.55	122.75
R(O1–C10)	1.354	1.354	1.354	A(O4–C19–C18)	117.54	122.74	117.55
R(O2–C8)	1.226	1.226	1.226	A(C17–C19–C18)	119.73	119.71	119.70
R(O3–C15)	1.362	1.362	1.362	Dihedral angle (°)			
R(O3–H28)	0.963	0.963	0.963	D(C10–O1–C7–C5)	1.10	−1.07	−1.05
R(O4–C19)	1.369	1.369	1.369	D(C10–O1–C7–C12)	−179.21	179.24	179.26
R(O4–H29)	0.963	0.963	0.963	D(C7–O1–C10–C6)	0.57	−0.45	−0.45
R(C5–C7)	1.400	1.400	1.400	D(C7–O1–C10–H20)	−179.09	179.02	179.01
R(C5–C8)	1.475	1.475	1.475	D(H28–O3–C15–C12)	−179.82	179.80	179.79
R(C5–C11)	1.405	1.405	1.405	D(H28–O3–C15–C16)	0.17	−0.17	−0.18
R(C6–C8)	1.480	1.480	1.480	D(H29–O4–C19–C17)	0.68	178.99	−0.47
R(C6–C9)	1.481	1.482	1.482	D(H29–O4–C19–C18)	−178.76	−0.45	178.91
R(C6–C10)	1.354	1.354	1.354	D(C8–C5–C7–O1)	−0.43	0.47	0.48
R(C7–C12)	1.393	1.393	1.393	D(C8–C5–C7–C12)	179.90	−179.86	−179.85
R(C9–C13)	1.402	1.404	1.402	D(C11–C5–C7–O1)	179.80	−179.81	−179.82
R(C9–C14)	1.404	1.402	1.404	D(C11–C5–C7–C12)	0.13	−0.14	−0.15
R(C10–H20)	1.082	1.082	1.082	D(C7–C5–C8–O2)	178.53	−178.78	−178.84
R(C11–C16)	1.380	1.380	1.380	D(C7–C5–C8–C6)	−1.63	1.41	1.37
R(C11–H21)	1.083	1.083	1.083	D(C11–C5–C8–O2)	−1.70	1.51	1.47
R(C12–C15)	1.388	1.388	1.388	D(C11–C5–C8–C6)	178.13	−178.29	−178.32
R(C12–H22)	1.082	1.082	1.082	D(C7–C5–C11–C16)	0.02	0.00	0.00
R(C13–C17)	1.391	1.389	1.391	D(C7–C5–C11–H21)	179.95	−179.94	−179.94
R(C13–H23)	1.081	1.085	1.081	D(C8–C5–C11–C16)	−179.75	179.71	179.71
R(C14–C18)	1.389	1.391	1.389	D(C8–C5–C11–H21)	0.18	−0.23	−0.23
R(C14–H24)	1.085	1.081	1.085	D(C9–C6–C8–O2)	2.95	−3.08	−3.17
R(C15–C16)	1.408	1.408	1.408	D(C9–C6–C8–C5)	−176.88	176.73	176.62
R(C16–H25)	1.086	1.086	1.086	D(C10–C6–C8–O2)	−177.08	177.45	177.53
R(C17–C19)	1.396	1.395	1.396	D(C10–C6–C8–C5)	3.10	−2.74	−2.68
R(C17–H26)	1.086	1.083	1.086	D(C8–C6–C9–C13)	−41.79	−141.23	38.94
R(C18–C19)	1.394	1.396	1.395	D(C8–C6–C9–C14)	138.88	39.97	−141.10
R(C18–H27)	1.083	1.086	1.083	D(C10–C6–C9–C13)	138.23	38.23	−141.77
Bond angle (°)				D(C10–C6–C9–C14)	−41.10	−140.56	38.19
A(C7–O1–C10)	118.91	118.92	118.92	D(C8–C6–C10–O1)	−2.76	2.45	2.40
A(C15–O3–H28)	110.01	109.99	109.99	D(C8–C6–C10–H20)	176.85	−176.96	−176.99
A(C19–O4–H29)	109.72	109.70	109.70	D(C9–C6–C10–O1)	177.22	−177.03	−176.91
A(C7–C5–C8)	121.04	121.06	121.08	D(C9–C6–C10–H20)	−3.17	3.56	3.70
A(C7–C5–C11)	117.68	117.67	117.67	D(O1–C7–C12–C15)	−179.85	179.87	179.87
A(C8–C5–C11)	121.27	121.26	121.25	D(O1–C7–C12–H22)	0.13	−0.14	−0.14
A(C8–C6–C9)	121.51	121.61	121.67	D(C5–C7–C12–C15)	−0.17	0.19	0.19
A(C8–C6–C10)	118.60	118.50	118.48	D(C5–C7–C12–C22)	179.82	−179.82	−179.82
A(C9–C6–C10)	119.89	119.88	119.85	D(C6–C9–C13–C17)	−178.14	−177.63	178.44
A(O1–C7–C5)	120.99	120.95	120.94	D(C6–C9–C13–H23)	2.40	4.05	−2.01
A(O1–C7–C12)	116.60	116.61	116.61	D(C14–C9–C13–C17)	1.21	1.21	−1.52
A(C5–C7–C12)	122.42	122.44	122.44	D(C14–C9–C13–H23)	−178.25	−177.11	178.02
A(O2–C8–C5)	122.09	122.00	121.97	D(C6–C9–C14–C18)	178.03	177.75	−178.32
A(O2–C8–C6)	123.53	123.57	123.60	D(C6–C9–C14–H24)	−3.54	−2.81	3.30
A(C5–C8–C6)	114.39	114.43	114.43	D(C13–C9–C14–C18)	−1.32	−1.09	1.65
A(C6–C9–C13)	121.37	120.80	121.47	D(C13–C9–C14–H24)	177.11	178.36	−176.74
A(C6–C9–C14)	120.79	121.42	120.78	D(C5–C11–C16–C15)	−0.12	0.09	0.09
A(C13–C9–C14)	117.84	117.77	117.75	D(C5–C11–C16–H25)	179.91	−179.92	−179.92
A(O1–C10–C6)	126.01	126.07	126.10	D(H21–C11–C16–C15)	179.95	−179.97	−179.97
A(O1–C10–H20)	110.45	110.38	110.36	D(H21–C11–C16–H25)	−0.03	0.02	0.02
A(C6–C10–H20)	123.54	123.55	123.54	D(C7–C12–C15–O3)	−179.95	179.95	179.95
A(C5–C11–C16)	121.08	121.08	121.08	D(C7–C12–C15–C16)	0.07	−0.09	−0.09
A(C5–C11–H21)	117.72	117.72	117.72	D(H22–C12–C15–O3)	0.07	−0.05	−0.04
A(C16–C11–H21)	121.20	121.20	121.20	D(H22–C12–C15–C16)	−179.92	179.92	179.92
A(C7–C12–C15)	118.43	118.42	118.42	D(C9–C13–C17–C19)	−0.36	−0.52	0.49
A(C7–C12–H22)	120.69	120.70	120.70	D(C9–C13–C17–H26)	179.87	−179.43	−179.78
A(C15–C12–H22)	120.88	120.88	120.88	D(H23–C13–C17–C19)	179.10	177.81	−179.06
A(C9–C13–C17)	120.94	121.68	120.96	D(H23–C13–C17–H26)	−0.67	−1.09	0.67
A(C9–C13–H23)	119.67	119.64	119.65	D(C9–C14–C18–C19)	0.56	0.29	−0.73
A(C17–C13–H23)	119.39	118.66	119.38	D(C9–C14–C18–H27)	179.49	−179.90	−179.53
A(C9–C14–C18)	121.63	120.96	121.69	D(H24–C14–C18–C19)	−177.88	−179.16	177.68
A(C9–C14–H24)	119.59	119.65	119.66	D(H24–C14–C18–H27)	1.05	0.65	−1.13
A(C18–C14–H24)	118.76	119.39	118.64	D(O3–C15–C16–C11)	−179.92	179.91	179.92
A(O3–C15–C12)	117.25	117.26	117.26	D(O3–C15–C16–H25)	0.06	−0.07	−0.07
A(O3–C15–C16)	122.12	122.11	122.11	D(C12–C15–C16–C11)	0.07	−0.05	−0.05
A(C12–C15–C16)	120.63	120.63	120.63	D(C12–C15–C16–H25)	−179.95	179.96	179.96
A(C11–C16–C15)	119.76	119.76	119.76	D(C13–C17–C19–O4)	−179.86	−179.77	179.85
A(C11–C16–H25)	120.44	120.43	120.43	D(C13–C17–C19–C18)	−0.44	−0.31	0.48
A(C15–C16–H25)	119.81	119.81	119.81	D(H26–C17–C19–O4)	−0.09	−0.84	0.12
A(C13–C17–C19)	120.24	119.61	120.27	D(H26–C17–C19–C18)	179.33	178.61	−179.25
A(C13–C17–H26)	119.75	121.17	119.71	D(C14–C18–C19–O4)	179.79	179.85	−179.76

Table 1 (*continued*)

Parameters	Optimized	Conformer C1	Conformer A1	Parameters	Optimized	Conformer C1	Conformer A1
A(C19–C17–H26)	120.01	119.22	120.01	D(C14–C18–C19–C17)	0.34	0.42	−0.36
A(C14–C18–C19)	119.60	120.26	119.61	D(H27–C18–C19–O4)	0.84	0.04	−0.93
A(C14–C18–H27)	121.18	119.72	121.16	D(H27–C18–C19–C17)	−178.61	−179.39	178.47

gen bonding, reactivity and structure activity relationship of molecules including biomolecules and drugs [61]. Electrostatic potential surfaces correlate with the dipole moment, electronegativity, partial charges and site of chemical reactivity of the molecule. The MEP has been used for predicting sites and relative reactivity towards electrophilic attack and in studies of biological recognition and hydrogen bonding interactions [62]. The 3D MEP of the title compound was calculated from optimized molecular structure by using B3LYP/6-311++G(d,p) and shown in Supplementary Fig. S4. The different values of the electrostatic potential at the MEP surface are represented by different colors; red, blue and green represent the regions of most negative, most positive and zero electrostatic potential, respectively. The negative electrostatic potential corresponds to an attraction of the proton by the aggregate electron density in the molecule (shades of red), while the positive electrostatic potential corresponds to the repulsion of the proton by the atomic nuclei (shades of blue). The negative (red color) regions of ESP were related to electrophilic reactivity and the positive (blue color) ones to nucleophilic reactivity. According to the result, negative region (red) is mainly over the carboxyl and hydroxyl group showing large activity. It can also be seen as hydroxyl group play an important role in the activity of diadzein particularly in the receptor binding, antioxidant activity, estrogenic, anti-estrogrnic activity and osteogenic activity [63–65]. The value of the electrostatic potential is largely responsible for the binding of a substrate to its receptor binding sites since the receptor and the corresponding legends recognize each other at their molecular surface [66,67].

UV–Vis spectroscopy

The reported UV absorption spectra of daidzein molecule was recorded in methanol solvent which show four absorption peaks at 238(sh), 249, 259(sh) and 303(sh) nm [37]. Comparison of observed and calculated (both for gas and solvent phase) UV–Vis spectra of daidzein is shown in Fig. 2. On the basis of a fully optimized ground state structure, the electronic spectra of daidzein were computed in the gas phase as well as in a methanol environment using TD-DFT method [38,39] and IEF-PCM model [40,41] employing B3LYP/6-31G functional. In an attempt to understand the nature of electronic transitions, positions of observed absorption peaks, calculated absorption peaks (λ_{max}'s), vertical excitation energies, oscillator strengths (f) and the assignments of the transitions of the daidzein molecule have been done and the results are shown in Table 2.

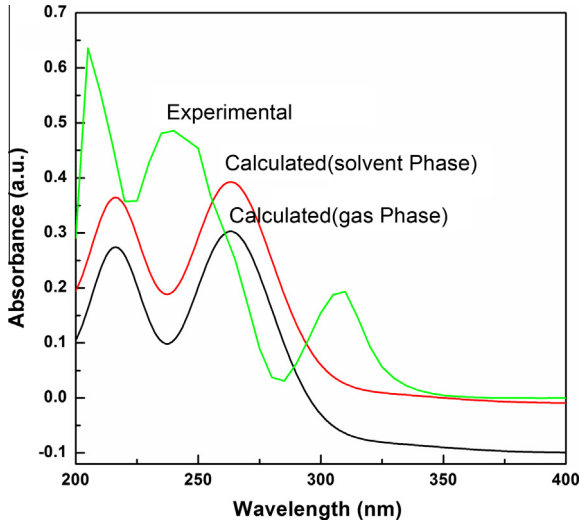

Fig. 2. Observed and calculated (both for gas and solvent phase) UV–Vis spectra of daidzein.

We have selected only four excitation transitions of UV–Vis for daidzein molecule. The strong bands observed at 303, 259, 249 and 238 nm and calculated at 280, 270, 246 and 222 nm in the gas phase, and at 324, 268, 240 and 224 nm in the solvent medium, respectively. The other transitions are weak enough to be observed experimentally. The first intense band at 303 nm corresponds to H to L+1 excitation in the gas phases and H to L excitation in solvent medium. The second absorption band at 259 nm originates from H−1 to L and H to L+1 in the gas phase and solvent medium, respectively. The third absorption band at 249 nm originates from H to L+2 and H to L+3 in the gas phase and solvent medium, respectively. Same as the fourth absorption band at 238 nm originates from H−3 to L+1 and H−1 to L+1 in the gas phase and solvent medium, respectively. However, the oscillator strength for the second transition is more than the others as shown in Table 2. This can be seen that the calculated values of peak position in solvent using IEF-PCM model [40,41] were closer to the experimental results as compared to the gas phase values. The analysis of the molecular orbital coefficients based on the optimized geometry indicate that daidzein has mainly p atomic orbitals and hence the electronic transitions corresponding to the electronic spectra are mainly of $\pi \rightarrow \pi^*$ type. The atomic molecular orbital plots for the frontier orbitals are plotted by GaussView [57].

The charge delocalization on the molecule is different for the different H and L energy levels. H is concerned as the ionization potential and L is concerned as the electron affinity. All H–L excitation transitions in both gas and solvent phase of daidzein molecule have been plotted as shown in Supplementary Figs. S5 and S6, respectively. In H, the charge is accumulated on both the rings (R2 and R3) whereas, very slight on R1 in both phases. In the both phase, the charge on H−1 is slightly shifted from R3 and no majority of charge is on R1 and slightly on R2. In the H−3, the charge density is uniformly distributed on all the three rings in the gaseous phase. In the solvent phases the charge on L is accumulated only on R1 and R2 where as in gaseous phase the charge is mainly on R3 and slightly on R2 and R1. In the L+1, the charge density is uniformly distributed on all the three rings and in the L+2 and L+3, the charge density is distributed on all the three rings (except on the one OH group) in the both phases. The above discussion helps to understand the charge concentration on frontier molecule in both the phases.

Mulliken atomic charges

The Mulliken procedure is the most common population analysis technique. Mulliken atomic charges (e), chemical potential (μ), electronegativity (χ), hardness (η), softness (S), global philicity (ω), HOMO–LUMO and their band gap (ΔE) are calculated by using DFT

Table 2
Electronic transitions, absorption peaks λ_{max} (in nm), oscillator strength (f) and assignments of the transitions of conformer C1.

Excited state	Experimental methanol		Calculated									
			Gas phase					Methanol				
	λ_{max} (nm)		λ_{max} (nm)	E (eV)	Oscillator strength (f)	Excitation transition	Transition type/ assignments	λ_{max} (nm)	E (eV)	Oscillator strength (f)	Excitation transition	Transition type/ assignments
	Reported	Observed										
1	303 (sh)	310	280	4.4287	0.1027	H → L+1	$\pi \rightarrow \pi^*$	324	3.8263	0.0272	H → L	$\pi \rightarrow \pi^*$
2	259 (sh)		270	4.5912	0.5370	H−1 → L	$\pi \rightarrow \pi^*$	268	4.6291	0.7864	H → L+1	$\pi \rightarrow \pi^*$
3	249	240	246	5.0347	0.0440	H → L+2	$\pi \rightarrow \pi^*$	240	5.1695	0.0351	H → L+3	$\pi \rightarrow \pi^*$
4	238 (sh)	205	222	5.5734	0.3683	H−3 → L+1	$\pi \rightarrow \pi^*$	224	5.5422	0.3997	H−1 → L+1	$\pi \rightarrow \pi^*$

for all the twelve conformers include initially optimized structure as mentioned in the Table 3. It can be seen very clearly from the Table 3 the negative atomic charges on oxygen atoms vary in the order of O2 > O4 > O3 > O1 which is applicable for all the conformers. Hence, it shows O2 has most negative charge compare to others. In the case of carbon atoms we found that C5, C6 and C9 atoms have positive electric charge and rest have negative electric charge which shows carbon atoms attached either with O or H atom have negative atomic charge. It is very clear from Table 3 that there is a large change in the Mulliken charges of the carbon atoms and this variation has pronounced effect on the reactivity of the conformers. The atomic charge on all the H atoms is positive in which H28 and H29 have highest positive charge on it due to the bonding with O3 and O4, respectively. The values of ΔE, μ, χ, η, S and ω is observed for all the conformers within a range −4.2399 to −4.1577, −3.9611 to −3.9453, 3.9453 to 3.9611, 2.0788 to 2.1199, 1.0394 to 1.0600 and 16.1847 to 16.6209, respectively.

Higher the value of ω results strong electrophilicity and measures the stabilization in energy when the system requires an addition charges from the environment whereas μ predicts the direction of charge transfer because an electrophile is capable of accepting electron from environment and its energy decrease when accepting electronic charge. On comparing both the conformers C1 and A1, A1 has the higher value of ω that shows its most electrophilic behavior and higher value of ΔE of A1 shows the low reactivity or high stability behavior. However, conformer B1 shows the most electrophilic behavior and most stable among all the conformers on the basis of ω and ΔE.

Table 3
Comparision of Mulliken atomic charges, Calculated HOMO, LUMO, band gap (ΔE), chemical potential (μ), electronegativity (χ), hardness (η), softness (S) and global electrophilicity (ω) of all conformers.

Atom no.	Mulliken atomic charge (e)											
	A1	A2	A3	B1	B2	B3	C1	C2	C3	D1	D2	D3
O1	−0.0526	−0.0527	−0.0525	−0.0525	−0.0585	−0.0557	−0.0522	−0.0525	−0.0554	−0.0667	−0.0576	−0.0561
O2	−0.2721	−0.2713	−0.2707	−0.2707	−0.2789	−0.2700	−0.2730	−0.2727	−0.2724	−0.2862	−0.2748	−0.2686
O3	−0.2115	−0.2116	−0.2111	−0.2111	−0.2113	−0.2138	−0.2115	−0.2116	−0.2140	−0.2359	−0.2113	−0.2141
O4	−0.2332	−0.2303	−0.2334	−0.2334	−0.2300	−0.2296	−0.2331	−0.2301	−0.2292	−0.2555	−0.2303	−0.2331
C5	1.9417	1.9511	1.9425	1.9425	1.3467	1.6495	1.9447	1.9412	1.6848	1.5761	1.4858	1.6600
C6	0.4643	0.4620	0.5231	0.5231	0.8011	0.4473	0.4819	0.4648	0.4126	0.8279	0.7643	0.4116
C7	−2.1559	−2.1108	−2.1667	−2.1667	−0.7855	−2.0105	−2.1538	−2.1030	−2.0165	−1.4872	−0.8923	−2.0451
C8	−0.4667	−0.4930	−0.5142	−0.5142	−0.5589	−0.4723	−0.4712	−0.4910	−0.4517	−0.3350	−0.5322	−0.4403
C9	1.2337	1.2514	1.2733	1.2733	1.3089	1.3594	1.2334	1.2589	1.3058	1.6104	1.2944	1.2991
C10	−0.0843	−0.0909	−0.0605	−0.0605	−0.6004	−0.1890	−0.0987	−0.1062	−0.2154	−0.4326	−0.6270	−0.1578
C11	0.2812	0.2686	0.2785	0.2785	−0.1032	0.2344	0.2795	0.2696	0.2282	0.0178	−0.0794	0.2478
C12	−0.3867	−0.4183	−0.3835	−0.3835	−0.6559	−0.0961	−0.3831	−0.4146	−0.0916	−0.2066	−0.6674	−0.0845
C13	−0.4003	−0.2213	−0.1362	−0.1362	−0.2407	−0.3139	−0.1533	−0.3603	−0.3182	−0.8298	−0.2624	−0.3181
C14	−0.2049	−0.4527	−0.5053	−0.5053	−0.3853	−0.3413	−0.4636	−0.2861	−0.3091	−0.8638	−0.4180	−0.2889
C15	−0.7156	−0.7121	−0.7274	−0.7274	−0.4695	−0.6457	−0.7145	−0.7081	−0.6407	−0.4940	−0.4998	−0.6534
C16	0.1246	0.1371	0.1276	0.1276	0.0232	0.0397	0.1247	0.1344	0.0390	0.0750	0.0555	0.0403
C17	−0.0267	−0.3260	−0.5428	−0.5428	−0.2067	−0.2097	−0.5325	−0.1811	−0.2037	0.1668	−0.2881	−0.0064
C18	−0.5423	−0.1693	−0.0025	−0.0025	−0.3370	−0.3357	−0.0319	−0.3528	−0.3572	0.1959	−0.1852	−0.5564
C19	−0.2981	−0.3122	−0.3199	−0.3199	−0.3283	−0.3440	−0.3001	−0.3050	−0.3191	−0.5397	−0.3378	−0.3264
H20	0.2225	0.2214	0.2147	0.2147	0.2045	0.2103	0.2226	0.2214	0.2189	0.1536	0.2040	0.2130
H21	0.1948	0.1959	0.1947	0.1947	0.2062	0.2015	0.1946	0.1959	0.2011	0.1585	0.2048	0.2011
H22	0.2128	0.2120	0.2125	0.2125	0.1991	0.1641	0.2128	0.2119	0.1645	0.1364	0.2004	0.1645
H23	0.1909	0.1924	0.1565	0.1565	0.1608	0.1557	0.1698	0.1677	0.1693	0.1442	0.1853	0.1851
H24	0.1674	0.1644	0.1847	0.1847	0.1875	0.1882	0.1917	0.1940	0.1952	0.1218	0.1560	0.1509
H25	0.1520	0.1522	0.1523	0.1523	0.1476	0.2061	0.1521	0.1521	0.2060	0.1136	0.1481	0.2058
H26	0.1446	0.2001	0.1898	0.1898	0.1342	0.1346	0.1895	0.1347	0.1337	0.1063	0.2014	0.1463
H27	0.1897	0.1349	0.1460	0.1460	0.2011	0.2012	0.1444	0.1997	0.1998	0.1286	0.1345	0.1903
H28	0.2648	0.2651	0.2646	0.2646	0.2662	0.2711	0.2648	0.2650	0.2712	0.2520	0.2661	0.2716
H29	0.2659	0.2640	0.2660	0.2660	0.2629	0.2641	0.2660	0.2639	0.2643	0.2479	0.2630	0.2659
HOMO	−6.0499	−6.0567	−6.0678	−6.0248	−6.0314	−6.0504	−6.0537	−6.0613	−6.0789	−6.0686	−6.0254	−6.0384
LUMO	−1.8584	−1.8541	−1.8454	−1.8672	−1.8633	−1.8508	−1.8571	−1.8527	−1.8399	−1.8535	−1.8652	−1.8565
ΔE	−4.1914	−4.2026	−4.2225	−4.1576	−4.1680	−4.1996	−4.1966	−4.2086	−4.2390	−4.2151	−4.1601	−4.1819
μ	−3.9542	−3.9554	−3.9566	−3.9460	−3.9474	−3.9506	−3.9554	−3.9570	−3.9594	−3.9611	−3.9453	−3.9475
χ	3.9542	3.9554	3.9566	3.9460	3.9474	3.9506	3.9554	3.9570	3.9594	3.9611	3.9453	3.9475
η	2.0957	2.1013	2.1112	2.0788	2.0840	2.0998	2.0983	2.1043	2.1195	2.1076	2.0801	2.0910
S	1.0479	1.0506	1.0556	1.0394	1.0420	1.0499	1.0492	1.0521	1.0596	1.0538	1.0400	1.0455
ω	3.7304	3.7227	3.7075	3.7451	3.7385	3.7164	3.7281	3.7204	3.6982	3.7223	3.7415	3.7261

NMR spectra

NMR spectroscopy is the most powerful tool for the analysis of organic compounds. The isotropic chemical shifts are very useful to provide the identification of the reactive ionic species and connectivity between the atoms in the molecule. Therefore, after optimization of the title molecule the chemical shifts of ^{1}H and ^{13}C are calculated by using gauge-including atomic orbital (GIAO) [58] approach with 6-311++G(d,p) basis set. The reported ^{1}H and ^{13}C chemical shifts were recorded in the DMSO (dimethyl sulphoxide) solvent [36] and compared with the calculated results. Chemical shifts in spectra are due to the shielding and deshielding of protons by the electrons. The isotropic shielding values, were used to calculate the isotropic chemical shifts δ with respect to TMS ($\delta^{x} = \delta^{TMS} - \delta^{c}$) the need of TMS is essential as a reference. The calculated isotropic chemical shielding for ^{1}H and ^{13}C are 31.84 and 183.68, respectively.

It can be seen from the Table 4 the ^{13}C chemical shifts are >100, which ensures the molecule to be organic [68,69]. The highest ^{13}C chemical shifts of C8, C15 and C19 are 174.8, 161.9 and 157.5, respectively, which shows the bonding with the electron attracting species (here O) as shown in Supplementary Fig. S1. The rest of the carbon atoms are within the range 115–157.2 ppm and match well with the calculated results. In order to compare the chemical shifts correlation graphs between the experimental and calculated chemical shifts are shown in Supplementary Fig. S7. The correlation graph follow the linear equation ($y = 1.00278x + 5.6676$); where y is the experimental ^{13}C NMR chemical shift, x is the calculated ^{13}C NMR chemical shift (δ in ppm). The value of correlation coefficient ($R^2 = 0.98557$) shows a good agreement between experimental and calculated results.

The highest ^{1}H chemical shift of H28 is observed at 9.62 and calculated at 4.07, this deviation clearly shows the intermolecular hydrogen bonding of hydroxyl group with the neighbouring molecules. We observed doublet for H26/H27 at 6.86 and H23/H24 at 7.44. Hence, from the above discussion it is clear higher the ppm value lower the electron donating property. The important aspect behind it is that electronegative (electron accepting) species decreases the shielding effect whereas electropositive (electron donating) increases the shielding effects. The intra and/or intermolecular interactions make the small difference between experimental and theoretical results due to the change of environment as the theoretical calculations are done on a single molecule.

Natural bond orbital analysis (NBO)

NBO analysis is the important approach for examining the hybridization, covalency effects and intramolecular charge transfer or conjugative interactions in polyatomic wave functions. First-order density matrix of the *ab initio* calculations was extracted to develop a unique set of atomic hybrids and bond orbitals which leads to "Lewis structure". It helps to understand the bonding in molecules. Delocalization of electron density between occupied, Lewis-type (bond or lone pair) NBO orbitals and formally unoccupied (antibond or Rydberg) non-Lewis NBO orbitals correspond to a stabilizing donor–acceptor interaction helps in the investigation of intermolecular/intramolecular interactions among bonds.

In the present work utilizing the second-order micro-disturbance theoretical analysis we have reported some of the electron donor, acceptor orbital and the interacting stabilization energy. The larger value of hyperconjugative interaction energy $E^{(2)}$, the more intensive is the interaction between the electron donors to electron acceptors [70–72]. The hyperconjugative interaction energy was deduced from the second-order perturbation approach

$$E^{(2)} = -n_{\sigma}[\langle\sigma|F|\sigma\rangle^{2}/\varepsilon_{\sigma^{*}} - \varepsilon_{\sigma}] = -n_{\sigma}[F_{ij}^{2}/\Delta E]$$

where $\langle\sigma|F|\sigma\rangle^{2}$ or F_{ij}^{2} is the Fock matrix element between i and j NBO orbital, ε_{σ} and $\varepsilon_{\sigma^{*}}$ are the energies of σ and σ^{*} NBO's, and n_{σ} is the population of the donor orbital. NBO analysis has been performed on the molecule at the B3LYP/6-31G level in order to elucidate the intramolecular, rehybridization and delocalization of electron density within the molecule, which are presented in Supplementary Table S2.

The most important interactions are from lone pair orbitals to the antibonding orbitals which give rise to the stabilization of the molecule. The most strong interaction among them is n(2)O1 → π*(C6–C10) and π*(C5–C7) leading to stabilization of 31.41 and 29.09 kcal/mol, respectively which are further stabilized into π*(C9–C14) and π*(C11–C16) with the stabilization energy of 38.45 and 275.15 kcal/mol, respectively. The other less intense interactions are due to O2, O3 and O4 shown in Supplementary Table S2. The interaction between n(2)O2 → σ*(C5–C8) and σ*(C6–C8) leading to the stabilization of 19.47 and 20.08 kcal/mol, respectively. The interaction between n(2)O3 → π*(C12–C15) and n(2)O4 → π*(C18–C19) leading to the stabilization of 30.73 and 29.51 kcal/mol, respectively and further stabilized into π*(C11–C16), π*(C9–C14) and π*(C13–C17) with the stabilized energy 242.16, 208.59 and 294.27 kcal/mol, respectively. These charge transfers are responsible for the structure activity of the system. The π*(C18–O19) of the NBO conjugated with π*(C13–C17) resulting to an enormous stabilization of 294.27 kcal/mol.

The another important intramolecular hyperconjugative interactions are formed by the orbital overlap between π(C–C) → π*(C–C) and bond orbitals, in ring R1 and Ring R3 which results in ICT (Intramolecular charge transfer) causing stabilization of the system within (~11–25 kcal/mol). These interactions are observed as increase in electron density (ED) in C–C antibonding orbital that weakens the respective bonds. The electron density of

Table 4
Experimental and theoretical, ^{1}H and ^{13}C NMR isotropic chemical shifts (with respect to TMS) of daidzein by DFT/B3LYP/6-311++(d,p) method.

Atom position	Experimental δ_H (J in Hz)	Theoretical δ_H	Atom position	Experimental δ_H (J in Hz)	Theoretical δ_H
H20	8.35 (1H, *s*)	8.20	C8	174.8	178.60
H21	8.04 (1H, *dd*, J = 8.7)	8.39	C9	122.6	131.25
H22	6.92 (1H, *d*, J = 1.6)	6.94	C10	152.9	157.66
H23	7.44 (2H, *d*, J = 8.4)	7.18	C11	127.3	135.56
H24	7.44 (2H, *d*, J = 8.4)	8.20	C12	102.1	107.63
H25	7.01 (1H, *d*, J = 8.7,1.6)	6.49	C13	130.1	134.03
H26	6.86 (2H, *d*, J = 8.4)	6.99	C14	130.1	139.05
H27	6.86 (2H, *d*, J = 8.4)	6.56	C15	161.9	167.50
H28	9.62 (1H, *br hump*)	4.07	C16	115.2	116.00
C5	116.7	125.57	C17	115.0	119.93
C6	123.5	132.68	C18	115.0	117.29
C7	157.2	165.12	C19	157.5	164.61

conjugated bond of benzene ring (~1.7e) clearly demonstrates strong delocalization.

NLO activity

Quantum chemical methods are presently used [73,74] for predicting the molecular NLO properties of different molecules. Hyperpolarizability is useful in understanding the relationship between the molecular structure and nonlinear optical properties. The dipole moment (μ), polarizability (α_0), anisotropy of polarizability ($\Delta\alpha$) and first hypepolarizability (β) of daidzein was calculated using B3LYP/6-311++G(d,p) basis set. The total static dipole moment (μ), the mean polarizability (α_0), the anisotropy of the polarizability ($\Delta\alpha$), and the mean first order hyperpolarizability (β) for daidzein were calculated by using the following equations [62]

$$\mu = (\mu_x^2 + \mu_y^2 + \mu_z^2)^{1/2}$$

$$\alpha_0 = 1/3(\alpha_{xx} + \alpha_{yy} + \alpha_{zz})$$

$$\Delta\alpha = 2^{-1/2}[(\alpha_{xx} - \alpha_{yy})^2 + (\alpha_{yy} - \alpha_{zz})^2 + (\alpha_{zz} - \alpha_{xx})^2]^{1/2}$$

$$\beta = [(\beta_{xxx} + \beta_{xyy} + \beta_{xzz})^2 + (\beta_{yyy} + \beta_{yzz} + \beta_{yxx})^2 + (\beta_{zzz} + \beta_{zxx} + \beta_{zyy})^2]^{1/2}$$

The Dipole moment (μ), and mean first hyperpolarizability (β) are calculated 2.3160 Debye and 1.2596×10^{-30} e.s.u., respectively shown in Supplementary Table S3. Total dipole moment of title molecule is approximately two times greater than urea and first hyperpolarizability of title molecule is approximately four times greater than urea [75,76]. Since the *x*, *y*, *z* component of α_0, $\Delta\alpha$ and β are reported in atomic unit (a.u.), the calculated values converted into electrostatic unit (e.s.u.) and the conversion factor of α and β in atomic unit are 1 atomic unit (a.u.) = 0.1482×10^{-24} electrostatic unit (e.s.u.) for α and 1 a.u. = 8.6393×10^{-33} e.s.u. for β.

Vibrational assignments

The title molecule has 29 atoms; hence it gives 81(3N−6) normal modes of vibrations. The molecular conformation obtained from the crystalline structure, as well as the one yielded by geometry optimization, exhibits no special symmetries and hence the molecule belongs to the C1 point group. As a consequence, all the 81 fundamental vibrations of the daidzein molecule belongs to the A irreducible representation, are both Raman and IR active. The vibrational spectrum was mainly determined by the modes of the free molecule observed at higher wavenumbers, together with the lattice (translational and vibrational) modes in the low wavenumber region.

DFT calculations yield Raman scattering amplitudes which cannot be taken directly to be the Raman intensities. The Raman scattering cross section, $\partial\sigma_j/\partial\Omega$, which are proportional to Raman intensity may be calculated from the Raman scattering amplitude and predicted wavenumbers for each normal mode using the relationship [77,78]

$$\frac{\partial\sigma_j}{\partial\Omega} = \left(\frac{2^4\pi^4}{45}\right)\left(\frac{(v_0 - v_j)^4}{1 - \exp\left[\frac{-hcv_j}{kT}\right]}\right)\left(\frac{h}{8\pi^2 c v_j}\right) S_j$$

where S_j and v_j are the scattering activities and the predicted wavenumbers, respectively of the *j*th normal mode, v_0 is the wavenumber of the Raman excitation line and *h*, *c* and *k* are universal constants. The calculated Raman and IR intensities were used to convolute each predicted vibrational mode with a Lorentzian line shape (FWHM = 8 cm^{-1}) to produce simulated spectra. Assignments have been made on the basis of relative intensities, energies, line shape and PED. All the vibrational bands have been assigned satisfactorily. Assigned wavenumbers of the intense vibrational modes calculated at the B3LYP level using basis set 6-311++G(d,p) along with their PED are given in Supplementary Table S4.

Vibrational wavenumber

Comparison of the wavenumbers calculated at B3LYP level with the observed spectra reveals an overestimation of the wavenumbers of the vibrational modes having neglected the anhormonicity present in a real system. Since the vibrational wavenumbers obtained from the DFT calculations are higher than the observed wavenumbers, they were scaled down by the wavenumber linear scaling procedure (WLS) [$v_{obs}/v_{cal} = (1.0087 - 0.000016 \times v_{cal})$ cm^{-1}] of Yoshida et al. [79] and a comparison was made with the observed values. The vibrational wavenumbers calculated with appropriate functionals are often in good agreement with the observed wavenumbers when the calculated wavenumbers are uniformly scaled with only one scaling factor [80,81]. All the calculated vibrational wavenumbers for both the conformers reported in this study are the scaled values and comparatively same.

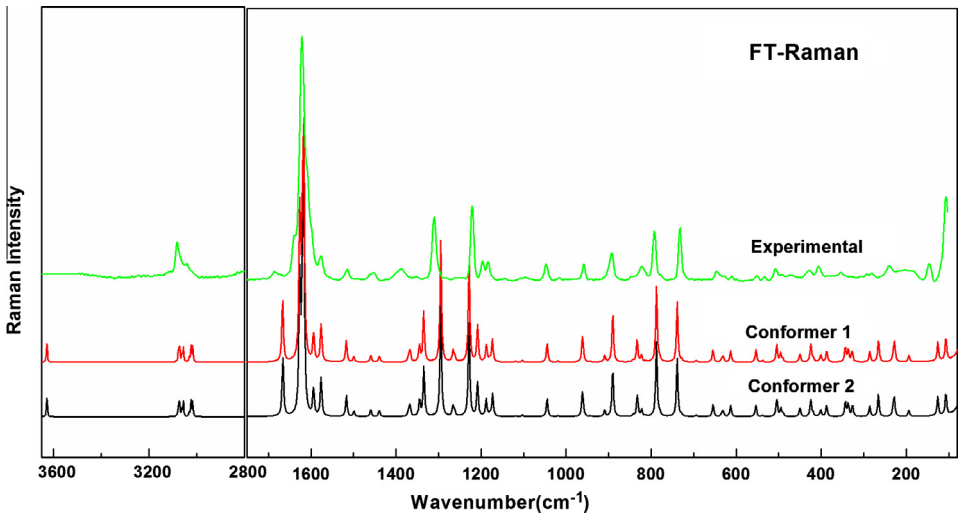

Fig. 3. Observed and calculated (scaled) Raman scattering spectra of daidzein in the region, 3200–2600 cm^{-1} and 1800–50 cm^{-1}.

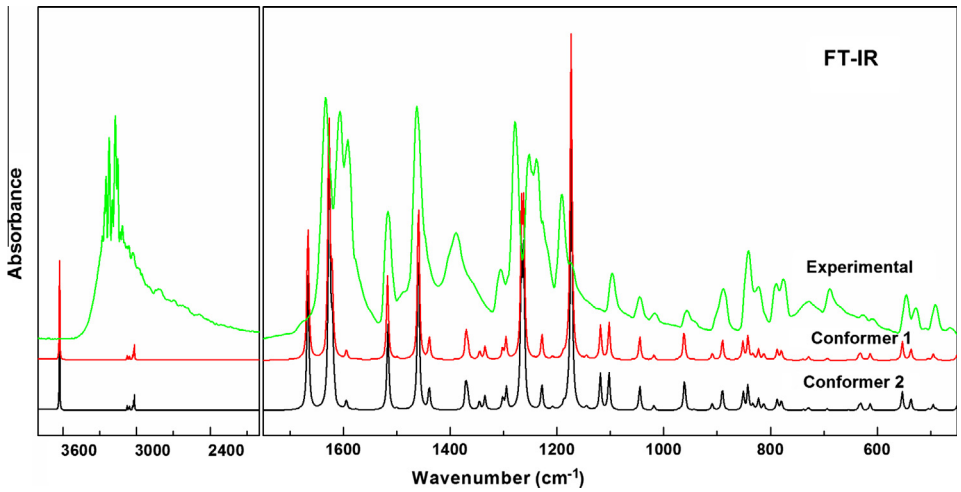

Fig. 4. Observed and calculated (scaled) IR absorption spectra of daidzein in the region, 3700–2800 cm^{-1} and 1800–400 cm^{-1}.

Comparison of observed and calculated (scaled) Raman and IR spectra of the two conformers C1 and A1 of daidzein is shown in Figs. 3 and 4, respectively. There are three rings in daidzein molecule as we can see in the Fig. 1(a and b) and hence we discuss the vibrational assignments of these three rings separately one by one.

Hydroxyl group vibrations

The hydroxyl group vibrations are likely to be the most sensitive to the environment, so the hydrogen bonded species show pronounced variation in the observables of a spectral band, such as band intensity and shape, frequency position of band maxima. The non-hydrogen bonded or free hydroxyl group absorbs strongly in the region 3600–3550 cm^{-1}, whereas the existence of hydrogen bond can lower the O–H stretching wavenumber to the 3550–3200 cm^{-1} region with an increase in the IR intensity and breadth [82]. The intense infrared absorption peak observed at 3173, 3223 cm^{-1} can be assigned to the stretching modes of OH group and calculated at 3626, 3628 cm^{-1} in the rings R1 and R3, respectively. The observed IR peak is shifted towards lower wavenumber region. The difference between observed and calculated values of O–H stretching vibration is due to the hydrogen bonding between OH groups and neighbouring molecules. Since our calculations are on isolated molecule whereas the observed spectra is for solid sample for bulk molecules. The deformation of hydroxyl group of both the rings (R3 and R1) is calculated at 1180 and 1173 cm^{-1} corresponding to the IR band at 1190 cm^{-1} and IR/Raman band at 1188/1183 cm^{-1}, respectively. In the conformer A1, the values of these modes are exactly same. Also, the mixed mode of OH bending, δ(O3H) of ring R1 for both the conformers, is calculated at the wavenumber 1208 cm^{-1} and assigned to the observed Raman band at 1220 cm^{-1}.

Ring R1 vibrations

The CH stretching of the ring is calculated at 3072/3062 cm^{-1} in both the conformers corresponding to the observed band at 3076/3061 cm^{-1} in the IR spectrum. The in-plane deformations of CH group are calculated at 1228 and 1103 cm^{-1} in the both conformers and reported at 1227/1221 and 1096/1096 cm^{-1} in the IR/Raman spectra, respectively. The observed medium intensity Raman peak at the 1221 cm^{-1} whereas IR peak at the 1096 cm^{-1} observed with low intensity. Out of three, two out-of-plane deformations of the CH group are calculated at 822 and 780 cm^{-1} and observed at 822/822 cm^{-1} and 775/791 cm^{-1} in the IR/Raman, respectively with the much lower intensity and matches well with both the conformers. Another out-of-plane deformation mode of the CH group is calculated at 971 cm^{-1} for both the conformers C1 and A1.

Total five CC stretching vibrations of the ring are calculated and three of them are calculated at 1627, 1459, 1370 cm^{-1} and observed at 1634, 1462 and 1389 cm^{-1} in the IR and 1638, 1453, 1387 cm^{-1} in the Raman spectrum, respectively. In conformer A1, the values of these modes are exactly same. The expected range of breathing mode of the substituted benzene rings generally found near the wavenumber 1000 cm^{-1} [83–85]. The low intense fourth mode is a mixed mode of R1[ν(CC)] and R3[oop(CH)] vibrations and calculated at 962 cm^{-1} that corresponds to the observed Raman peak at 959 cm^{-1} with much lower intensity. The fifth mode of CC stretching vibration of the ring is calculated at 1576 cm^{-1} for both the conformers and matches nicely at the peak at 1576 cm^{-1} in Raman spectrum.

The stretching mode ν(O3C) for both the conformers are calculated at wavenumber 1262 cm^{-1} corresponds to the observed IR band at 1252 cm^{-1}. The asymmetric deformations of the ring are calculated to be 613/495 cm^{-1} and observed at 609/610 cm^{-1} and 492/492 cm^{-1} in IR/Raman spectrum, respectively. The torsion modes calculated at the wavenumber 490 and 450 cm^{-1} corresponds to the observed band at 490 and 463 cm^{-1} in the IR spectra.

Ring R2 vibrations

The CH stretching vibration of the ring is calculated at 3075 cm^{-1} and assigned to the IR/Raman peak at 3078/3081 cm^{-1}. An intense stretching mode ν(CC) is calculated at 1617 cm^{-1} in both conformers corresponding to the observed band at 1607/1621 cm^{-1} in the IR/Raman spectra with the same intensity. The stretching mode of C=O of the ring is calculated at 1667 cm^{-1} and assigned to weak Raman band at 1686 cm^{-1} where as in the conformer A1, the calculated value is at 1666 cm^{-1}. The stretching vibration of ring COC with low contribution is calculated at the 1228 cm^{-1} in both the conformer and corresponds to the observed peak at 1227/1221 cm^{-1} in the IR/Raman spectra. In-plane bending of C=O is calculated at 613 cm^{-1} with very low contribution for both the conformers and corresponds to the peak at 609/610 cm^{-1} in the IR/Raman spectra. However, this mode is also found in a mixed mode of deformation of rings R1& R2. Absorption peak (In plane deformation) of δ_{in}(C=O) is calculated at 343 cm^{-1} in mixed mode having the contribution of δ_{in}(C=O), δ_{in}(C6C9) of ring R2 and δ_{in}(C19O), δ_{in}(C9C6) of ring R3 that corresponds to observed band at the 354 cm^{-1} in the Raman spectra.

The out of plane deformation of CH group is calculated at 909 cm^{-1} in both conformers and assigned to the Raman band at 894 cm^{-1}. The asymmetric deformation of the ring is calculated at 553 cm^{-1} in conformer C1 which corresponds to the observed band at 546/550 cm^{-1} in the IR/Raman spectra. The trigonal defor-

mation of the ring is calculated at 890 cm^{-1} in both the conformers and observed at 887/892 cm^{-1} in the IR/Raman spectrum. The ring torsion was calculated at 126 cm^{-1} for both the conformers and observed at 145 cm^{-1} in the Raman spectra.

Ring R3 vibrations

Vibrations of benzene ring are separated into two parts (i) modes which are predominantly CH stretching vibrations and (ii) the modes which predominantly involve CC vibrations [82]. The ν(CH) wavenumbers of the ring are predicted at 3078, 3032, 3017 cm^{-1} corresponding to the observed IR bands at 3080, 3032, 2991 cm^{-1} and Raman peaks at 3083, 3040, 3000 cm^{-1}, respectively whereas in the case of conformer A1 it is calculated to be 3079, 3032 and 3017 cm^{-1}. The ring stretching ν(CC) and breathing modes are calculated at 1621 and 1045 cm^{-1} corresponding to the observed strong peaks at 1632/1623 cm^{-1} and at 1045/1048 cm^{-1} as weak intensity peak in the IR/Raman spectrum, respectively. The other CC stretching vibrations is calculated at 1439 cm^{-1} but not observed in the IR/Raman spectra whereas two ν(CC) modes are calculated at 1594 and 1302 cm^{-1} corresponds to the observed IR band at 1591 and 1306 cm^{-1}, respectively. Another CC stretching mode is calculated 1345 cm^{-1} that corresponds to the observed Raman band at 1353 cm^{-1}.

Vibrations involving CH in-plane bending are found throughout the region 1000–1300 cm^{-1}. The CH out-of-plane bending vibrations give rise to bands in the region 700–1000 cm^{-1} [84–86]. However, in substituted benzene rings the C–H in-plane bending is found throughout the region 1500–1100 cm^{-1} and these in-plane bending vibrations interact sometimes strongly with ν(CC) vibrations of the ring. The contribution of CC stretching is more dominant than CH bending in higher region and vice versa. The bend-stretch modes from 1500 to 1300 cm^{-1} are affected by stronger substituent bonds. With increasing substitution, the CH deformations appear to interact more readily with lower frequency ring modes [84,85]. The four modes of in-plane deformations of the ring CH are calculated at the 1517, 1345, 1187 and 1118 cm^{-1}. The first two modes at the 1517 and 1345 cm^{-1} are strongly coupled with the ring CC stretching (have about 40% contributions from ring CC) as such have higher values. However, the last two modes are dominantly CH in-plane bending vibration. Out of four, two in-plane bending of ring CH is calculated at 1517, 1187 cm^{-1} and observed at 1516, 1192 as medium intensity band in the IR spectra and at 1515, 1196 cm^{-1} in the Raman spectrum with very low intensity and matches well for both the conformers in the wavenumber as well as intensity. Two other in-plane deformations of ring CH are calculated at 1345 and 1118 cm^{-1} corresponding to the Raman band at the 1353 and 1108 cm^{-1}, respectively.

Out-of-plane vibration oop(CH) of both conformers are calculated at 960 and 842 cm^{-1} in low intensity and assigned at 957, 841 cm^{-1} in the IR spectra and at 957, 845 cm^{-1} in the Raman spectra with the same intensity.

Puckering mode of ring is calculated at 728 cm^{-1} corresponds to the observed band at 729/732 cm^{-1} in IR/Raman spectrum, respectively. The asymmetric deformation of the ring is calculated to be 631 cm^{-1} for the both conformers and observed at the 627 cm^{-1} in the IR and 627 cm^{-1} in the Raman spectra.

Conclusion

In the present study the experimental (vibrational) and theoretical (computational) analysis of the possible conformations of the title molecule has been reported. The optimized geometry, wavenumber and intensity of the vibrational bands of possible conformers were obtained by density functional theory (DFT) employing B3LYP using 6-311++G(d,p) basis set. Detailed assignments of the vibrational spectra of the most stable conformers have been made with the aid of theoretically predicted vibrational frequencies. Finally, the calculations were applied to simulate infrared and Raman spectra of the title compound which showed good agreement with observed spectra. Mulliken population analysis on atomic charges of various conformers is also calculated. Electrostatic potential surface is plotted for predicting the size, shape, charge density distribution and structure activity relationship. The UV spectrum has been recorded in methanol solution and compared with the calculated results in gas phase as well as in the methanol environment (IEF-PCM model) using TD-DFT method with 6-31G basis set and it matches well with the solvent phase. The H–L energy gap of possible conformers has been calculated for comparing their chemical activity and charge transfer within the molecule. The NMR analysis confirms the aromaticity of the molecule, electronegative groups, and H-bonding in the molecule. The NBO analysis reveals O3 and O4 has the most intensive interaction between the Lewis acceptor and Lewis donor that results the stability of the molecule. NLO analysis predict the nonlinearity of the molecule which is helpful for the studying the nonlinear properties. To the best of our knowledge this is the first time where the conformational study is done and a complete vibrational assignment along with PED is being presented for the title molecule. The noted discrepancies between experimental and theoretical results are due to the fact that the calculations were done on the single molecule in gaseous state neglecting the intermolecular interactions.

Acknowledgements

A.S. thanks CSIR (New Delhi) for financial assistance in the form of a Research Associateship (R.A.). S.S. is thankful for the support from the UGC under BSR meritorious fellowship scheme.

Appendix A. Supplementary material

Supplementary data associated with this article can be found, in the online version, at http://dx.doi.org/10.1016/j.saa.2013.10.045.

References

[1] R. Maurya, D.K. Yadav, G. Singh, B. Bhargavan, P.S.N. Murthy, M. Sahai, M. Singh, Bioorg. Med. Chem. Lett. 19 (2009) 610–613.
[2] I. Orhan, B. Ozcelik, M. Kartal, S. Aslan, B. Sener, Acta Biol. Cracoviensia Series Bot. 49 (2007) 61–68.
[3] A.L. Ososki, E.J. Kennelly, Phytother. Res. 17 (2003) 845–869.
[4] J.J.B. Anderson, Nutr. Res. Rev. 12 (1999) 75–116.
[5] H. Adlercreutz, W. Mazur, P. Bartels, V. Elomaa, S. Watanabe, K. Wahala, M. Landstrom, E. Lundin, A. Bergh, J.E. Damber, P. Aman, A. Widmark, A. Johansson, J.X. Zhang, G. Hallmans, J. Nutr. 130 (2000) 658–659.
[6] S.O. Mueller, S. Simon, K. Chae, M. Metzler, K.S. Korach, Toxicol. Sci. 80 (2004) 14–25.
[7] W.N. Ratna, Life Sci. 71 (2002) 865–877.
[8] M.B.R. Larrea, A.R. Mohan, G. Paganga, N.J. Miller, G.P. Bolwell, C.A.R. Evans, Free Radical Res. 26 (1997) 63–70.
[9] L. Markiewicz, J. Garey, H. Adlercreutz, E. Gurpide, J. Steroid Biochem. Mol. Biol. 45 (1993) 399–405.
[10] J. Chen, H. Lin, M. Hu, Pharmacol. 55 (2005) 159–169.
[11] W. Miltyk, C.N. Craciunescu, L. Fischer, R.A. Jeffcoat, M.A. Koch, W. Lopaczynski, C. Mahoney, R.A. Jeffcoat, J. Crowell, J. Paglieri, S.H. Zeisel, Am. J. Clin. Nutr. 77 (2003) 875–882.
[12] H. Tsuchiya, M. Nagayama, T. Tanaka, M. Furusawa, M. Kashimata, H. Takeuchi, BioFactors 16 (2002) 45–56.
[13] D. Urban, W. Irwin, M. Kirk, M.A. Markiewicz, R. Myers, M. Smith, H. Weiss, W.E. Grizzle, S. Barnes, J. Urol. 165 (2001) 294–300.
[14] F. Marotta, G.S. Mao, T. Liu, D.H. Chui, A. Lorenzetti, Y. Xiao, P. Marandola, Ann. NY Acad. Sci. 1089 (2006) 276–281.
[15] B.J. Boersma, T.D. Alessandro, M.R. Benton, M. Kirk, L.S. Wilson, J. Prasain, N.P. Botting, S. Barnes, V.M.D. Usmar, R.P. Patel, Free Radical Biol. Med. 35 (2003) 1417–1430.
[16] H.H. Lai, G.C. Yen, Biosci. Biotechnol. Biochem. 66 (2002) 22–28.
[17] D. Park, T. Huang, W.H. Frishman, Cardiol Rev. 13 (2005) 13–17.
[18] D.G. Gruen, D.K. Silverstein, J. Nutr. 131 (2001) 1202–1206.

[19] I.W. Potocka, K. Okuda, T.J. Acosta, A. Korzekwa, W. Pilawski, D.J. Skarzynski, Prostaglandins Other Lipid Mediat. 78 (2005) 202–217.
[20] A.N. Lam, M. Demasi, M.J. James, A.J. Husband, C. Walker, Nutr. Cancer 49 (2004) 89–93.
[21] D.R. Doerge, H.C. Chang, J. Chromatogr. B: Anal. Technol. Biomed. Life Sci. 777 (2002) 269–279.
[22] G.T. Liu, Y.L. Zheng, W.H. Chen, J. Chen, Z.K. Han, J. Nanjing Agric. Univ. 22 (1999) 69–72.
[23] H. Adlercreutz, T. Yamada, K. Wahala, S. Watanabe, Am. J. Obst. Gynecol. 180 (1999) 737–743.
[24] D.R. Miller, G.M. Lee, P.F. Maness, J. Neurochem. 60 (1993) 2134–2144.
[25] P. Wang, C.J. Jeng, C.L. Chien, S.M. Wang, Biochem. Biophys. Res. Commun. 366 (2008) 393–400.
[26] T.C. Ma, A. Campana, P.S. Lange, H.H. Lee, K. Banerjee, J.B. Bryson, L. Mahishi, S. Alam, R.J. Giger, S. Barnes, J.S.M. Morris, D.E. Willis, J.L. Twiss, M.T. Filbin, R.R. Ratan, J. Neurosci. 30 (2010) 739–748.
[27] L. Zhao, Q. Chen, R.D. Brinton, Exp. Biol. Med. (Maywood) 227 (2002) 509–519.
[28] V. Crupi, D. Majolino, M.R. Mondello, P. Migliardo, V. Venuti, J. Pharm. Biomed. Anal. 29 (2002) 1149–1152.
[29] G. Fini, J. Raman Spectrosc. 35 (2004) 335–337.
[30] H.S. Nalwa, S. Miyata, Nonlinear Optics of Organic Molecules and Polymers, CRC Press, Boca Raton, FL, 1997.
[31] A.A. Kaminskii, Laser Photon. Rev. 1 (2007) 93–177.
[32] J. Hulliger, A.A. Kaminshii, H.J. Eichler, Adv. Funct. Mater. 11 (2001) 243–250.
[33] R.T. Bailey, G.H. Bourhill, F.R. Cruickshank, D. Pugh, J.N. Sherwood, G.S. Simpson, K.B.R. Verma, J. Appl. Phys. 75 (1) (1994) 489–492.
[34] C. Bosshard, R. Spreiter, L. Degiorgi, P. Gunter, Phys. Rev. B 66 (2002) 205107. 9 pages.
[35] P. Hohenberg, W. Kohn, Phys. Rev. B 136 (1964) 864–871.
[36] A. Pelter, R.S. Ward, R.J. Bass, J. Chem. Soc. Perkin Trans. 1 (1978) 666–668.
[37] S. Chansakaow, T. Ishikawa, K. Sekine, M. Okada, Y. Higuchi, M. Kudo, C. Chaichantipyuth, Planta Med. 66 (2000) 572–575.
[38] M.E. Casida, K.C. Casida, D.R. Salahub, Int. J. Quan. Chem. 70 (1998) 933–941.
[39] R.E. Stratmann, G.E. Scuseria, M.J. Frisch, J. Chem. Phys. 109 (1998) 8218–8224.
[40] E. Cances, B. Mennucci, J. Tomasi, J. Chem. Phys. 107 (1997) 3032–3041.
[41] B. Mennucci, J. Tomasi, J. Chem. Phys. 106 (1997) 5151–5158.
[42] J. Chocholousova, V.V. Spirko, P. Hobza, J. Chem. Phys. 6 (2004) 37–41.
[43] M. Montejo, A. Navarro, G.J. Kealey, J. Vazquez, J.J.L. Gonzalez, J. Am. Chem. Soc. 126 (2004) 15087–15095.
[44] F.D. Proft, P. Geerlings, Phys. Chem. Chem. Phys. 6 (2004) 24–248.
[45] A. Tanwar, S. Pal, J. Chem. Sci. 117 (2005) 497–505.
[46] M.J. Frisch, G.W. Trucks, H.B. Schlegel, G.E. Scuseria, J.R. Cheeseman, M.A. Robb, G. Scalmani, V. Barone, B. Mennucci, G.A. Petersson, H. Nakatsuji, M. Caricato, X. Li, H.P. Hratchian, A.F. Izmzylov, J. Bloino, G. Zheng, J.L. Sonnenberg, M. Hada, M. Ehara, K. Toyota, R. Fukuda, J. Ishida, M. Hasegawa, T. Nakajima, Y. Honda, O. Kitao, H. Nakai, T. Vreven, J.A. Montgomery Jr., J.E. Peralta, F. Ogliaro, M.Bearpark, J.J. Heyd, E. Brothers, K.N. Kudin, V.N. Staroverov, R. Kobayashi, J. Normand, A.Raghavachari, A. Rendell, J.C. Burant, S.S. Iyengar, J. Tomasi, M. Cossi, N. Rega, J.M. Millan, M. Klene, J.E. Knox, J.B. Cross, V. Bakken, C. Adamo, J. Jaramillo, R. Gomperts, R.E. Stratmann, O. Yazyev, A.J. Austin, R. Cammi, C. Pomelli, J.W. Ochterski, R.L. Martin, K. Morokuma, V.G. Zakrzewski, G.A. Voth, P. Salvador, J.J. Dannerberg, S. Dapprich, A.D. Daniels, J. Farkas, B. Foresman, J.V.Ortiz, J. Cioslowski, D.J. Fox, GAUSSIAN 09, Revision, Gaussian, Inc., Wallingford, CT, 2009.
[47] C.T. Lee, W.T. Yang, R.G. Parr, Phys. Rev. B 37 (1988) 785–789.
[48] R.G. Parr, W. Yang, Density Functional Theory of Atoms and Molecules, Oxford University Press, New York, 1989.
[49] A.D. Becke, J. Chem. Phys. 98 (1993) 5648–5652.
[50] G.A. Petersson, M.A. Allaham, J. Chem. Phys. 94 (1991) 6081–6090.
[51] G.A. Petersson, A. Bennett, T.G. Tensfeldt, M.A. Allaham, W.A. Shirley, J. Mantzaris, J. Chem. Phys. 89 (1988) 2193–2218.
[52] P. Pulay, G. Fogarasi, F. Pang, J.E. Boggs, J. Am. Chem. Soc. 101 (1979) 2550–2560.
[53] G. Fogarasi, X. Zhou, P.W. Taylor, P. Pulay, J. Am. Chem. Soc. 114 (1992) 8191–8201.
[54] J.M.L. Martin, C.V. Alsenoy, Gar2ped, University of Antwerp, 1995.
[55] G.A. Zhurko, D.A. Zhurko, Chemcraft. <http://www.chemcraftprog.com>.
[56] N. Sundaraganesan, K.S. Kumar, C. Meganathan, B.D. Joshua, Spectrochim. Acta A 65 (2006) 1186–1196.
[57] A. Frisch, A.B. Nielson, A.J. Holder, GaussView User Manuual, Gaussian Inc., Pittsburgh, PA, 2000.
[58] R. Ditchfield, J. Chem. Phys. 56 (1972) 5688.
[59] R. Ditchfield, Mol. Phys. 27 (1974) 789–807.
[60] K. Wolinski, J.F. Hinton, P. Pulay, J. Am. Chem. Soc. 112 (1990) 8251–8260.
[61] S. Chidangil, M.K. Shukla, P.C. Mishra, J. Mol. Model. 4 (1998) 250–258.
[62] N. Gunay, H. Pir, D. Avci, Y. Atalay, J. Chem. (2013) 16 (Article ID 712130).
[63] Z. Huang, F. Fang, J. Wang, C.W. Wong, FEBS Lett. 584 (2010) 22–26.
[64] K. Dwiecki, G. Neunert, P. Polewski, K. Polewski, J. Photochem. Photobiol. B: Biol. 96 (2009) 242–248.
[65] Q. Jiang, F.P. Stewart, S. Elliott, J. Driver, L.V. Rhodes, Q. Zhang, S. Zheng, D. Bhatnagar, S.M. Boue, B.M.C. Burow, J. Sridhar, C. Stevens, J.A. McLachlan, T.E. Wiese, M.E. Burow, G. Wang, J. Med. Chem. 53 (2010) 6153–6163.
[66] H. Kobinyi, G. Folkers, Y.C. Martin, 3D QSAR in drug design, Recent Advances, vol. 3, Kluwer Academic Publishers, 1998.
[67] S. Moro, M. Bacilieri, C. Ferrari, G. Spalluto, Curr. Drug Discov. Technol. 2 (2005) 13–21.
[68] H.O. Kalinowski, S. Berger, S. Brawn, Carbon 13 NMR spectroscopy, John Wiley & Sons, Chichester, 1988.
[69] K. Pihlajer, E. Kleinpeter (Eds.), Carbon 13 Chemical Shifts in Structure and Pectrochemical Analysis, VCH Publishers, Deerfield Beach, 1994.
[70] F. Weinhold, C.R. Landis, Valency and Bonding: A Natural Bond Orbital Donor Acceptor Perspective, Cambridge University Press, New York, 2005.
[71] F. Weinhold, C.R. Landis, Chem. Educ. Res. Pract. Eur. 2 (2001) 91–104.
[72] A.E. Reed, L.A. Curtiss, F. Weinhold, Chem. Rev. 88 (1988) 899–926.
[73] R.T. Bailey, T.J. Dines, M.C. Tedford, J. Mol. Struct. 992 (2011) 52–58.
[74] A. Subhashini, R. Kumarvel, S. Leela, H.S. Evans, D. Sastikumar, K. Ramamurthi, Spectrochim. Acta A 78 (2011) 935–941.
[75] L. Sinha, O. Prasad, V. Narayan, S.R. Shukla, Mol. Simul. 37 (2011) 153–163.
[76] S. Sebastian, N. Sundaraganesan, B. Karthikeiyan, V. Srinivasan, Spectrochim. Acta A 78 (2011) 590–600.
[77] P.L. Polavarapu, J. Phys. Chem. 94 (1990) 8106–8112.
[78] G.A. Guirgis, P. Klaboe, S. Shen, D.L. Powell, A. Gruodis, V. Aleksa, C.J. Nielsen, J. Tao, C. Zheng, J.R. Durig, J. Raman Spectrosc. 34 (2003) 322–336.
[79] H. Yoshida, K. Takeda, J. Okamura, A. Ehara, H. Matsurra, J. Phys. Chem. A 106 (2002) 3580–3586.
[80] M.W. Wong, Chem. Phys. Lett. 256 (1996) 391–399.
[81] A.P. Scott, L. Radom, J. Phys. Chem. 100 (1996) 16502–16513.
[82] N.B. Colthup, L.H. Daly, S.E. Wiberley, Introduction to Infrared and Raman Spectroscopy, Academic Press, New York, 1990.
[83] Y. Yamakita, Y. Isogai, K. Ohno, J. Chem. Phys. 124 (2006) 104301–104318.
[84] J.R. Scherer, Spectrochim. Acta 19 (1963) 601–610.
[85] J.R. Scherer, Spectrochim. Acta 21 (1965) 321–339.
[86] G. Varsanyi, Assignments for Vibrational Spectra of Seven Hundred Benzene Derivatives, vols. 1 and 2, Academic Kiado, Budapest, 1973.